ISSN 1063-7842, Technical Physics, 2021, Vol. 66, No. 1, pp. 98–102. © Pleiades Publishing, Ltd., 2021.
Russian Text © The Author(s), 2021, published in Zhurnal Tekhnicheskoi Fiziki, 2021, Vol. 91, No. 1, pp. 105–109.

ELECTROPHYSICS

A Study of the Spatial Charge Effect on 2-MeV Proton Beam Transport in an Accelerator-Based Epithermal Neutron Source

T. A. Bykov[a,b], D. A. Kasatov[a,b], Ia. A. Kolesnikov[a,b], A. M. Koshkarev[a,b], A. N. Makarov[a,b], G. M. Ostreinov [a,b], E. O. Sokolova[a,b], S. Yu. Taskaev[a,b,*], and I. M. Shchudlo[a,b]

[a] *Budker Institute of Nuclear Physics, Siberian Branch, Russian Academy of Sciences, Novosibirsk, 630090 Russia*
[b] *Novosibirsk State University, Novosibirsk, 630090 Russia*
**e-mail: taskaev@inp.nsk.su*

Received March 16, 2020; revised May 22, 2020; accepted July 8, 2020

Abstract—A neutron source composed of a tandem accelerator with vacuum insulation and a lithium target is used to develop the boron neutron capture therapy and other applications. The dependence of the proton beam size on the target surface on the beam current is measured with thermocouples inserted inside the target and with a infrared camera. It is found that there is no appreciable influence of the spatial charge on the proton beam transport to a distance of 5 m from the accelerator to the target, which simplifies the neutron source operation.

DOI: 10.1134/S1063784221010047

INTRODUCTION

At the Budker Institute of Nuclear Physics, Siberian Branch, Russian Academy of Sciences, there is an accelerator source of epithermal neutrons [1] that was designed for the development of a promising method for the treatment of malignant tumors—boron neutron capture therapy (BNCT) [2]. The source is composed of a tandem accelerator with vacuum insulation to produce a stationary proton beam, a lithium target to generate neutrons due to the threshold reaction ^{7}Li(p,n)^{7}Be [3], and an epithermal neutron beam shaping assembly [4]. The neutron source is used to carry out biological research in the field of BNCT [5, 6], to measure the content of impurities in ceramic samples by activation analysis [7], and to prepare the radiation testing of optical fibers by fast neutrons [8]. Earlier we used a wire scanner to measure the dependence of the profile and current of the negative hydrogen ion beam injected into the tandem accelerator with vacuum insulation on the residual gas pressure and found the influence produced by the spatial charge on the ion beam transport [9]. In order to offset the spatial charge effect, the focusing lens force is changed so that to focus the negative hydrogen ion beam on the accelerator input, controlling the beam size, and to make it parallel in the stripping target of the accelerator, while controlling the target heating.

The purpose of this paper is to determine whether the spatial charge influences the proton beam during its transport from the accelerator to the target. It is proposed to measure the transverse size of the proton beam on the target as a function of the proton beam current.

1. EXPERIMENTAL FACILITY SCHEMATIC

The neutron source scheme is presented in Fig. 1; its detailed description is given in [1]. The proton beam is obtained in the following way. A beam of negative hydrogen ions with an energy under 25 keV is extracted from ion source *1* and deflected by an angle of 15° in the magnetic field of the ion source. Then the negative hydrogen ion beam is focused by magnetic lens *2* on accelerator input *3* [9] and is accelerated to the energy of 1 MeV. In gas stripping target *4* mounted inside the high-voltage electrode of the accelerator, negative hydrogen ions are transformed into protons that are accelerated to the energy of 2 MeV by the same potential 1 MV. The proton current is varied by the discharge current and the extraction voltage of ion source *1*. The proton energy is calculated by measuring the voltage of the high-voltage potential using a resistive voltage divider and is calibrated to the threshold of the reaction of neutron generation ^{7}Li(p,n)^{7}Be equal to 1.882 MeV. In order to transport protons from the accelerator to neutron-generating target *11* located horizontally at a distance of 5 m, the beam transport channel with the cross section of 60 mm is used. It is equipped with corrector *7* to correct the direction of the proton beam propagation; bending magnet *8* to deflect the proton beam downward by the angle of 90°; scanner *10* to sweep the proton beam over the target surface; three cooled copper diaphragms *5* with

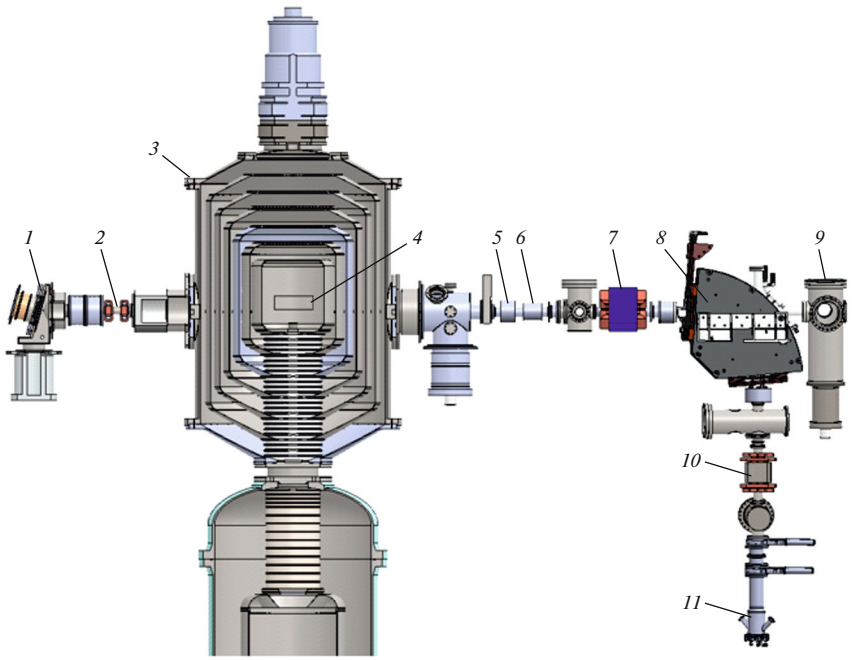

Fig. 1. Schematic of the accelerator-based epithermal neutron source: (*1*) source of negative hydrogen ions, (*2*) magnetic lens, (*3*) tandem accelerator with vacuum insulation, (*4*) stripping target, (*5*) cooling diaphragm, (*6*) non-destructive DC current transformer, (*7*) corrector, (*8*) bending magnet, (*9*) second diagnostic chamber with the insertable Faraday cup, (*10*) scanner, and (*11*) lithium neutron generating target.

thermocouples to measure the proton beam position and to prevent burning-through of the vacuum chamber by the beam; three Faraday cups with thermocouples, which are inserted to control current and the proton beam position; and a non-destructive DC current transformer NPCT-CF4 (Bergoz Instruments, France)

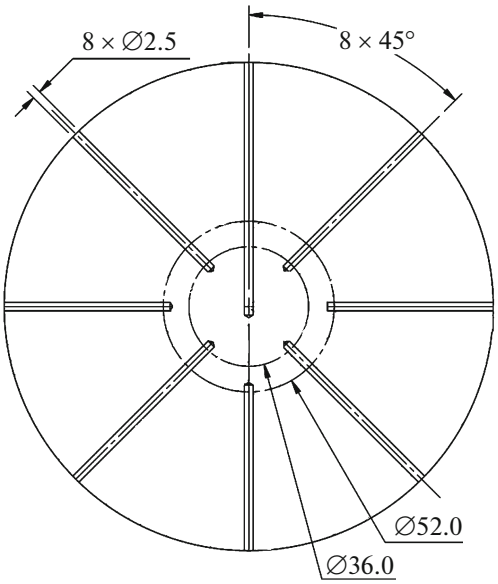

Fig. 2. Schematic of thermocouple arrangement in the target copper disk.

for continuous measurement of the proton beam current. The typical residual gas pressure in the channel is 0.5 mPa.

The neutrons are generated during the threshold reaction ^{7}Li(p,n)^{7}Be, where 2-MeV protons interact with lithium deposited on a copper heat removal substrate that is efficiently cooled by water. The copper substrate is similar to the one described in [3] and has been used for 10 years for neutron production: it is made in the form of a disk 143 mm in diameter and 8 mm in thickness. The substrate is flat on the side of the proton beam; on the other side, it has four spiral-shaped double-turn 3-mm-deep channels for water coolant with an input temperature between 22.5 and 22.8°C. There are eight holes drilled on the lateral side surface of the copper disk at a distance of 2.5 mm from the flat surface, in which the thermocouples are inserted (Fig. 2). Four thermocouples are placed uniformly in azimuth at a distance of 18 mm from the center of the disk. The other four thermocouples are positioned uniformly in azimuth with a shift by 45° relative to the first thermocouples; one of them is at the disk center and the other three are at a distance of 26 mm from the disk center. After the thermocouples were placed, the holes were sealed with high-temperature cement.

An FLIR T650SC infrared camera (FLIR Systems Inc., United States) mounted on a branch pipe with a barium fluoride window at an angle of 45° to the target surface is used to monitor the position and size of the

proton beam. A Optris CT Laser 3ML SF pyrometer (Optris, Germany) mounted on the second branch pipe is used to control the surface temperature of the target. The proton beam current is measured by a nondestructive DC current transformer NPCT-CF4 and a resistive voltage divider connected to the target that is electrically insulated from the facility. Glycerin pressure gages (WIKA, Germany), PT2415 pressure sensors (IFM, Germany), SV7614 flowmeters (IFM, Germany), and water temperature sensors are placed on the panel connected to the target with hoses on inch in diameter and 5.7 m in length.

2. MEASUREMENT RESULTS AND DISCUSSION

A proton beam with an energy of 2 MeV, current from 0.48 to 3.2 mA, and lateral dimension of 1 cm [10] is obtained from the vacuum insulated tandem accelerator and directed to the target. The proton beam size on the target is determined by the output electrostatic lens of the accelerator, the bending magnet, and the spatial charge action. The behavior of axisymmetric uncompensated beam envelope $R(z)$ under the action of its own field is described by the equation $\frac{d^2R(z)}{dz^2} = \frac{K}{R(z)}$, where z is the longitudinal coordinate and $K = \frac{I_0 e}{2\pi m\varepsilon_0(\beta\gamma c)^3}$ is the generalized perveance of the beam. This nonlinear second order differential equation has the following solution [11]:

$$Z = \frac{R_0}{\sqrt{2K}} F(\rho),$$

where R_0 is the initial radius of the beam, $\rho = \frac{R(z)}{R_0}$, and $F(\rho) = \int_1^\rho \frac{dy}{\sqrt{\ln y}}$. According to the solution of this equation, the beam radius on the target increases by 1.2 times at 0.5 mA and by 1.6 times at 3 mA. The additional increase in the beam size on the target may be due to the action of a spatial charge in the focus area of the bending magnet. If the electric charge of protons in the beam transport channel is offset by the electric charge of electrons that emerge during the proton interaction with residual gas, the spatial charge effect is absent. In this case, the size of the proton beam on the target is determined only by the output electrostatic lens of the accelerator and the bending magnet and is independent of the proton beam current. Within this study, lithium was not evaporated on the target and the scanner for sweeping the proton beam over the surface of the target was not turned on. The target was cooled by water flowing through cooling channels, and the measured water discharge was 15.1 L/min.

Measuring the profile of a stationary continuous proton beam with a high power density of up to 20 kW/cm^2 is a challenging task that has to be solved. In the horizontal part of the transport channel, the proton beam profile was measured using the following four techniques based on:

(I) propagation of the boundary of the blister production region with the increase in fluence of the 2-MeV protons implanted in copper [10];

(II) spatial distribution of activation of the lithium layer of the neutron-generating target by the radioactive isotope ^{7}Be produced within the threshold reaction ^{7}Li(p,n)^{7}Be [12];

(III) dependence of the current that has passed through the cooled diaphragm inserted inside the bending magnet on the magnetic field of the bensing magnet;

(IV) propagation of the boundary of the lithium melting region with the increase in the proton beam power.

In all cases, the measured profile is described quite well by the Gaussian distribution. On the lithium target placed in the vertical part of the beam transport channel, the profile of the proton beam can be determined by heating the lithium target surface. It was found that the Optris CT Laser 3ML SF pyrometer underestimates the temperature due to its wide measurement range, 19 mm, and the lack of technical capability to identify the emission factor lower than 0.1 that is typical for the polished copper surface. On the contrary, the FLIR T650SC infrared camera overestimates temperature readings due to a nonthermal glow caused by the copper luminescence under the action of high-energy protons, which was described in a study of blistering [10] as a variation in the emissivity of the copper surface exposed to a proton beam. In addition, the camera software does not allow digitizing temperature measurement results without using the built-in autocalibration algorithm. Reliable temperature measurement was performed by thermocouples used earlier in the study of the heat removal from the target during its heating [13].

In Fig. 3, the typical image of the FLIR T650SC infrared camera (FLIR, United States) is shown stretched vertically by a factor of $\sqrt{2}$. The dotted circle 30 mm in diameter is superimposed on the image. It is shown that the proton beam heats the area inside the diameter of 30 mm. Note that the light dots in the image are heated small metal droplets that fall on the target from above, when to the proton beam touches the vacuum chamber walls at the increase in the accelerator voltage, and heated blisters that emerge during the implantation of 2-MeV protons into copper [10]. The light oval around the proton beam shown by the dotted line is not related to heating, but is the reflection of infrared radiation of the target from the walls of the cylindrical branch pipe on which the camera is mounted. Further, during the study, the infrared cam-

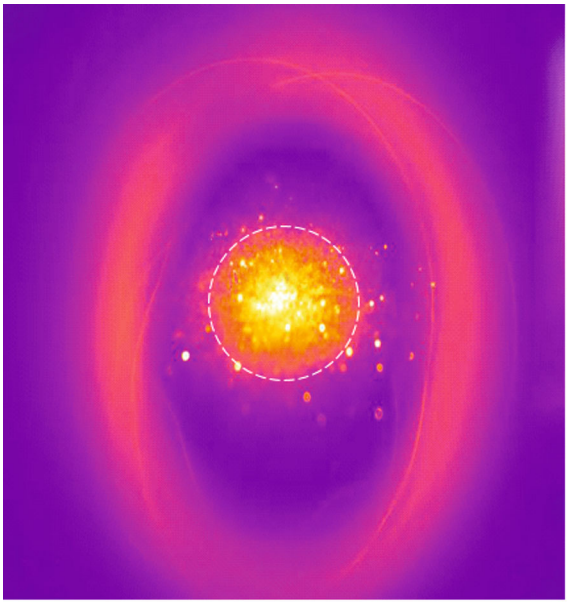

Fig. 3. Image obtained from the infrared camera during the target irradiation by a proton beam with a current of 1.4 mA. The dashed circle denotes the diameter of 30 mm.

era images were used to correct the proton beam position on the target.

Thermocouples inserted into the copper disk of the lithium target were used to measure the temperature when the target was irradiated by a proton beam with a current that varied from 0.48 to 3.2 mA. The results of temperature measurement averaged over the corresponding number of thermocouples are shown in Fig. 4. The temperature of the target surface (copper disk) can be determined as

$$T = \Delta T_{Cu} + \Delta T_{w-liq} + \Delta T_{liq} + T_{liq},$$

where ΔT_{Cu} is the temperature gradient on copper, $\Delta T_{w\ -\ liq}$ is the temperature difference between the cooled wall and the liquid, ΔT_{liq} is the mean heating of the coolant, and T_{liq} is the initial temperature of the coolant.

The path projected range of a 2-MeV proton in copper is 19 μm [14], much less than the copper disk thickness, and so it may be assumed that the proton beam heats only the surface. In this case, the temperature gradient from the disk surface to the cooling channel can be estimated as follows: $\Delta T_{Cu} = qh_{Cu}/\lambda_{Cu}$, where q is the heating power density, $h_{Cu} = 5$ mm and $\lambda_{Cu} = 400$ W m^{-1} K^{-1} are the thickness and the thermal conductivity coefficient of copper.

The heat transfer from the solid wall to the coolant is carried out by the convection heat exchange that is efficient at the turbulent fluid flow. In Fig. 4, it is shown that the temperature grows linearly with the increase in heating, which indicates that the wall is cooled by the turbulent water flow without boiling. If an even more efficient mode of heat removal by turbulent water flow with bubble boiling were implemented, the temperature would remain constant without regard to the increase in heating [13]. In the mode of heat removal by turbulent water flow without boiling, the temperature gradient between the cooled wall and the coolant $\Delta T_{w\ -\ liq}$ is determined as $\Delta T_{w\ -\ liq} = P/(\alpha S)$, where P is the heating power transferred, S is the heat exchange surface area, and α is the heat transfer coefficient determined by the hydrodynamic mode of liquid flow and its thermodynamic properties [15].

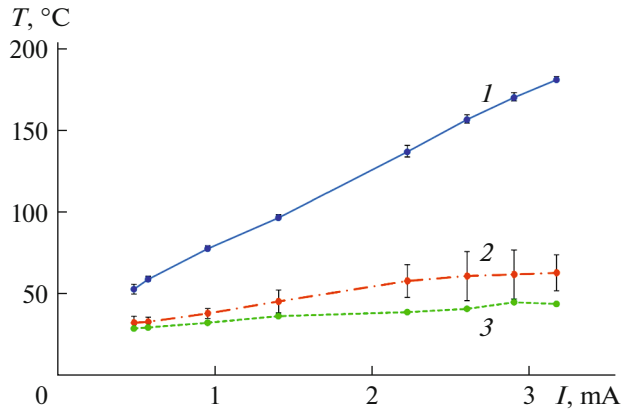

Fig. 4. Target temperature as a function of the proton beam current: (*1*) at the center, (*2*) at a distance of 18 mm from the center, and (*3*) at a distance of 26 mm from the center.

Heat is removed by water. So, at the exit from the target, the water is heated by $\Delta T_{liq} = P/(C_pQ)$; here, P is the heating power, and C_p and Q are the heat capacity of water and water flowrate.

The linear dependence on the heating power characterizes all three components of the temperature gradient: ΔT_{Cu}, $\Delta T_{w\ -\ liq}$, and ΔT_{liq}. Consequently, the target heating is proportional to the proton beam power, so the measured temperature distribution can be used to recover the proton beam power density profile. We present the radial distribution of power, and thus of temperature, as the Gaussian distribution: $T(r) = \Delta T_0 \exp(-r^2/r_0^2) + T_{liq}$, where $\Delta T_0 = \Delta T_{Cu} + \Delta T_{w\ -\ liq} + \Delta T_{liq}$ is the temperature increase at the maximum heating power density, i.e., at the proton beam center; r_0 is the proton beam radius. Then, measuring temperature at the center T_0 and at the known radius T_r ($r_t =$ 18 or 26 mm), we determine the proton beam radius as $r_0 = r_t/(\ln A)^{1/2}$, where $A = (T_0 - T_{liq})/(T_r - T_{liq})$. The result of recovery of the proton beam radius as a function of current is shown in Fig. 5.

It is shown that the proton beam radius determined in this way is slightly different, depending on whether we take the readings from thermocouples placed on the radius of 18 mm or thermocouples placed on the radius of 26 mm. This difference can be explained by the fact that the shape of the proton beam is slightly different from that of the Gaussian.

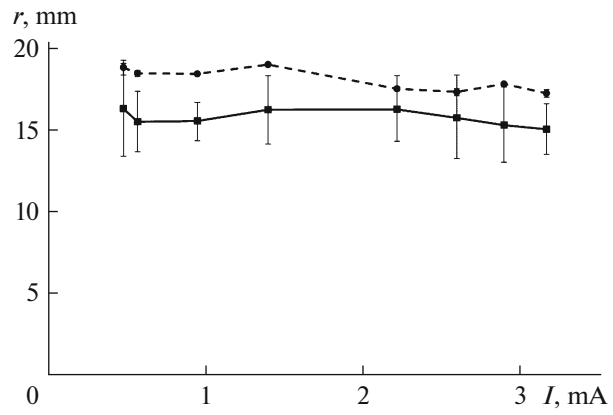

Fig. 5. Proton beam radius as a function of the beam current. Dashed line is plotted according to the data from the thermocouples positioned on a 26-mm radius. Solid line is plotted according to the data from the thermocouples positioned on an 18-mm radius.

The main result of the study is that the size of the proton beam on the target does not depend on the proton beam current in the range from 0.48 to 3.2 mA; the proton beam diameter is 33 ± 5 mm. The lack of dependence of the proton beam size on the target surface on the beam current indicates that there is no noticeable effect of the spatial charge on the proton beam transport from the accelerator to the target. This fact simplifies the configuration of the proton beam transport channel, since it does not require installing quadrupole lenses, and simplifies considerably the proton beam obtaining in a wide current range, which is important when performing studies on the facility.

CONCLUSIONS

In the accelerator-base neutron source of the Budker Institute of Nuclear Physics, Siberian Branch, Russian Academy of Sciences, a 2-MeV proton beam is transported for a distance of 5 m from the accelerator to a lithium neutron-generating target. The proton beam size on the target surface is measured as a function of the beam current by thermocouples inserted into the target and by an infrared camera. It is found that the proton beam diameter is 33 ± 5 mm and is independent of the current in the range from 0.48 to 3.2 mA. This fact indicates that there is no significant influence of the spatial charge on the proton beam transport from the accelerator to the target, which simplifies the configuration of the beam transport channel and ensures the reliability of obtaining the beam in a wide current range.

FUNDING

This study was supported by the Russian Science Foundation (project no. 19-72-30005) and the Budker Institute of Nuclear Physics, Siberian Branch, Russian Academy of Sciences.

CONFLICT OF INTEREST

The authors declare that they have no conflicts of interest.

REFERENCES

1. S. Yu. Taskaev, Phys. Part. Nucl. **46** (6), 956 (2015). https://doi.org/10.1134/S1063779615060064
2. *Neutron Capture Therapy. Principles and Applications*, Ed. by W. Sauerwein, A. Wittig, R. Moss, and Y. Nakagawa (Springer, Berlin, 2012). https://doi.org/10.1007/978-3-642-31334-9
3. B. Bayanov, V. Belov, and S. Taskaev, J. Phys.: Conf. Ser. **41**, 460 (2006). https://doi.org/10.1088/1742-6596/41/1/051
4. L. Zaidi, M. Belgaid, S. Taskaev, and R. Khelifi, Appl. Radiat. Isot. **139**, 316 (2018). https://doi.org/10.1016/j.apradiso.2018.05.029
5. E. Sato, A. Zaboronok, T. Yamamoto, K. Nakai, S. Taskaev, O. Volkova, L. Mechetina, A. Taranin, V. Kanygin, T. Isobe, B. Mathis, and A. Matsumura, J. Radiat. Res. **59** (2), 101 (2018). https://doi.org/10.1093/jrr/rrx071
6. S. Taskaev, Phys. Part. Nucl. **50** (5), 569 (2019). https://doi.org/10.1134/S1063779619050228
7. A. Shoshin, A. Burdakov, M. Ivantsivskiy, S. Polosatkin, M. Klimenko, A. Semenov, S. Taskaev, D. Kasatov, I. Shchudlo, A. Makarov, and N. Davydov, IEEE Trans. Plasma Sci. **48** (6), 1474 (2020). https://doi.org/10.1109/TPS.2019.2937605
8. D. A. Kasatov, A. M. Koshkarev, A. N. Makarov, G. M. Ostreinov, S. Yu. Taskaev, and M. Shchudlo, Instrum. Exp. Tech. **63** (5), 611 (2020). https://doi.org/10.1134/S0020441220050152
9. T. A. Bykov, D. A. Kasatov, Ia. A. Kolesnikov, A. M. Koshkarev, A. N. Makarov, Yu. M. Ostreinov, E. O. Sokolova, I. N. Sorokin, S. Yu. Taskaev, and I. M. Shchudlo, Instrum. Exp. Tech. **61** (5), 713 (2018). https://doi.org/10.1134/S0020441218050159
10. A. Badrutdinov, T. Bykov, S. Gromilov, Y. Higashi, D. Kasatov, I. Kolesnikov, A. Koshkarev, A. Makarov, T. Miyazawa, I. Shchudlo, E. Sokolova, H. Sugawara, and S. Taskaev, Metals **7** (12), 558 (2017). https://doi.org/10.3390/met7120558
11. M. D. Gabovich, *Physics and Technology of Plasma Ion Sources* (Atomizdat, Moscow, 1972) [in Russian].
12. T. Bykov, N. Goloshevskii, S. Gromilov, D. Kasatov, Ia. Kolesnikov, A. Koshkarev, A. Makarov, A. Ruktuev, I. Shchudlo, E. Sokolova, and S. Taskaev, Nucl. Instrum. Methods Phys. Res., Sect. B **481**, 62 (2020). https://doi.org/10.1016/j.nimb.2020.08.010
13. B. Bayanov, V. Belov, V. Kindyuk, E. Oparin, and S. Taskaev, Appl. Radiat. Isot. **61**, 817 (2004). https://doi.org/10.1016/j.apradiso.2004.05.032
14. H. H. Andersen and J. F. Ziegler, *Hydrogen Stopping Powers and Ranges in All Elements* (Pergamon, New York, 1977), Vol. 3.
15. S. S. Kutateladze, *Fundamentals of Heat Transfer* (Academic, New York, 1963).

Translated by N. Semenova